JOURNAL OF MATERIALS SCIENCE 32 (1997) 5271–5278

Microstructural characteristics of shock consolidated 2124 Al alloy compacts

K. SIVAKUMAR, K. SATYA PRASAD, T. BALAKRISHNA BHAT
Defence Metallurgical Research Laboratory, Hyderabad-500 058, India
P. RAMAKRISHNAN
Indian Institute of Technology, Powai, Bombay-400 076, India

2124 alloy powders have been compacted using explosive compaction. The effect of process parameters like explosive pad thickness and impact energy imparted to the powders on the microstructure and hardness across the cross-section of the compact have been investigated. When the thickness of the explosive pad was increased to 9.5 mm, three distinct microstructures with different hardness values were found across the cross-section of the compact. The size and shape of the θ phase precipitates were different in the fine grained structure when compared with that of the original particles and triple point junctions. Central porosity and pipe formation were observed when the thickness of the explosive pad was increased beyond 14.5 mm. Variation in the microstructure of the compact across the cross-section disappeared when the diameter of the compact was increased from 11 to 25 mm.

1. Introduction

The consolidation of powdered materials by dynamic compaction is receiving much attention, particularly with the recognition of the ability to consolidate rapidly solidified metastable powders without affecting their special microstructural features [1–6]. Therefore, it is of interest to study the effects of dynamic compaction on rapidly solidified microstructures. Some studies on air atomized aluminium powder compacted using two stage gas guns [7] indicated anisotropic deformation around the surface of the particles. In large melted pools, dispersed oxides were seen. Fine grain size and entrapped microporosity were also found and were attributed to rapid freezing. In the shock consolidation of aluminium and Al–1.4 wt % Co powders, defect substructures exhibited extensive recovery from heating associated with dynamic consolidation [8]. In the present study, microstructural variations occurring during explosive compaction of atomized 2124 aluminium alloy powders have been investigated.

2. Experimental procedure

The arrangement for explosive compaction is shown in Fig. 1. The compaction was carried out in 10 and 25 mm diameter aluminium tubes. One end of the tube was closed by a plug and the powder was vibratory packed to uniform density along the length of the tube. Subsequently, the tube was closed by a second plug and the tube assembly centrally located inside a cylindrical plastic container. The annular cavity between the metallic tube and the plastic container was packed to a uniform density with trimonite, an explosive powder. Detonation of the explosive was carried out from one end of the assembly in the vertical position. This produced a convergent cylindrical shock wave that collapsed the tube and compacted the powder.

The particle size of the 2124 powder used in the experiments was 45 μm. The explosive pad thickness between the metallic tube and plastic container was varied from 5 to 22 mm. The impact energy imparted to the powder varied from 177 to 4545 MJ m^{-3}, when calculated using the equation given by Hegazy and Blazynski [9]. The method of calculating the impact energy imparted to the system has been given elsewhere [10]. Other experimental details are given in Table I. After compaction, the compacts were cut for microstructural and hardness studies. Optical metallography specimens were prepared by standard polishing techniques and etched with Kellars' reagent. Transmission electron microscopy (TEM) specimens were prepared by the twin jet electron polishing technique using an electrolyte consisting of 30% HNO_3 in methanol at 15 V. TEM studies were made using a Philips EM 430 T microscope using an accelerating voltage of 300 kV.

3. Results

The microstructure of the starting material is shown in Fig. 2. With a 5 mm thick explosive pad 97.54% theoretical density was obtained. The microstructure

0022–2461

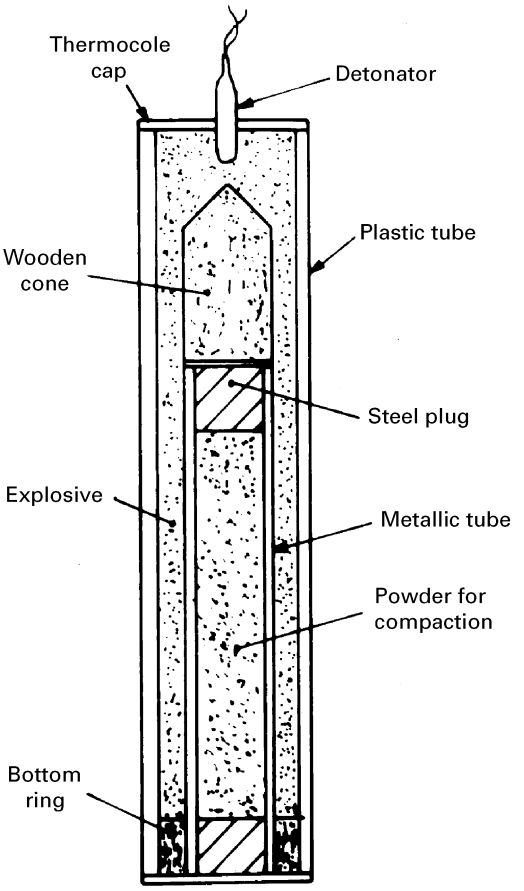

Figure 1 Experimental setup for explosive compaction.

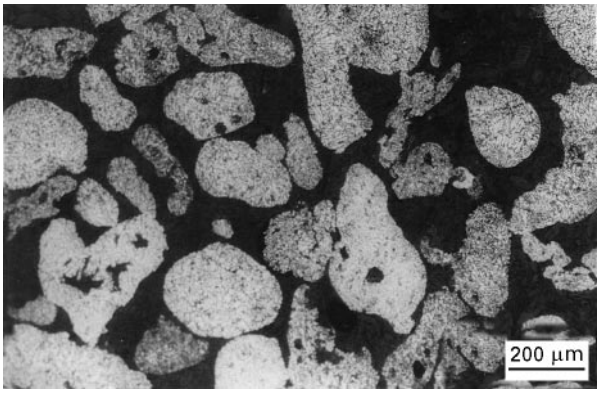

Figure 2 Microstructure of 2124 Al powder.

of the compact produced, shown in Fig. 3, shows almost uniform structure except at the centre, where a region 2 mm in diameter having different microstructure occurs. The microstructure at the periphery

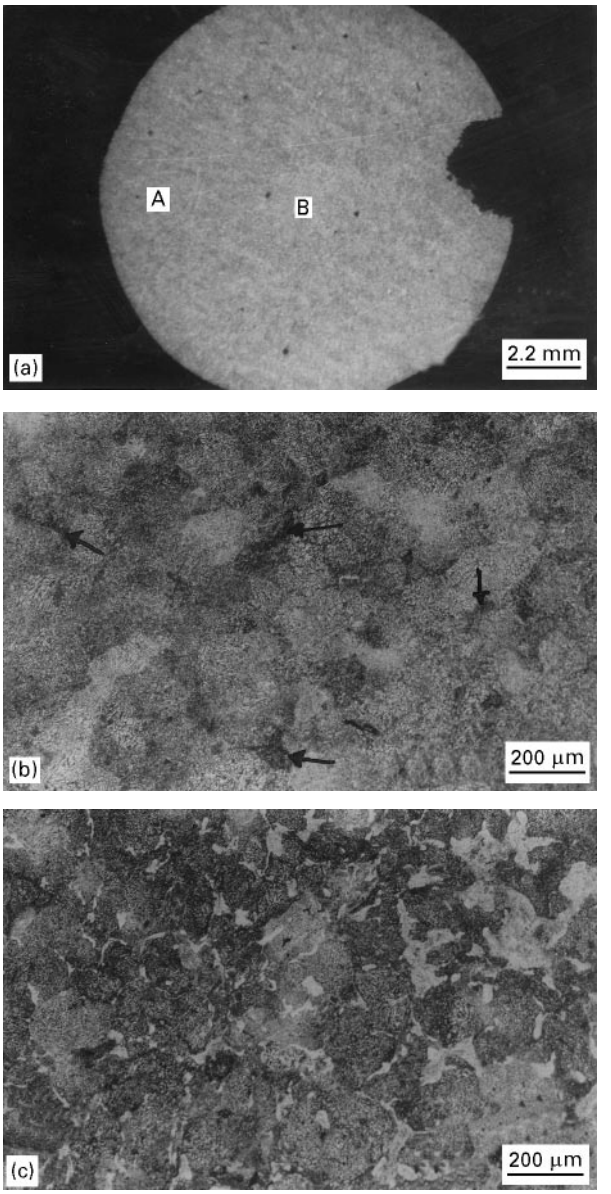

Figure 3 (a) Microstructure of the 2124 Al compact produced by the 5 mm thick explosive pad, showing different structures across the cross-section. (b) periphery (A) and (c) centre (B).

of the compact showed a fine dendrite structure similar to that of the original powder. The central regions of the compact showed a dual structure with new white non-etching areas amidst the original dendritic structures. At the periphery of the compact, prior particle boundaries completely vanished and we found a new type of structure showing up as black patches.

TABLE I Experimental details of explosive compaction of 2124 Al powder

Sample No.	Tube diameter (mm)		Explosive pad thickness (mm)	E_m/P_m	Impact energy ($MJ\,m^{-3}$)	Pressure (GPa)	R (E_m/T_m)	% theoretical density
	Inner	Outer						
1	11	16	5.0	1.78	177	0.70	1.08	97.54
2	11	16	9.5	4.11	919	1.45	2.49	95.67
3	11	16	14.0	7.14	2062	2.16	4.31	Central porosity
4	11	16	22.0	14.20	4545	3.37	8.59	Pipe formation
5	25	32	8.5	1.43	220	1.33	1.386	98.00

E_m = Explosive mass
P_m = Powder mass
T_m = Metallic tube mass

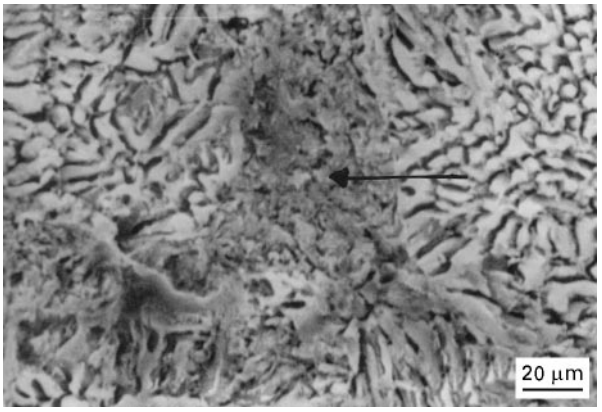

Figure 4 SEM micrograph showing remelted zones at the triple point junctions at the periphery of the compact produced by the 5 mm thick explosive pad.

The microstructure in these black patches is extremely fine as shown by the arrow marks in the scanning electron micrograph (Fig. 4).

The variation in the microstructure is even more significant when the explosive pad thickness is increased to 9.5 mm. Across the cross-section of the compact, we find three distinct regions (Fig. 5). At the periphery, the structure is similar to the initial dendritic structure. When we move in by about 3 mm from the periphery towards the centre, we find a dual structure showing a mixture of the original dendritic structure and non-etching white regions, similar to the one obtained at the central region of the compact using the 5 mm thick explosive pad. The dual structure appears as a 1 mm thick ring as shown by the arrows in the figure. At the centre of the compact, a cellular network type structure is observed. This region contains some porosity and cracks too. The microhardness in these three different regions, i.e. the regions with original dendritic structure, non-etching white areas and the central areas with cellular structure, were found to be 80, 92 and 58 Vickey's Pyramid Number (VPN), respectively.

Fig. 6 shows the effect on the microstructure when the explosive pad thickness is increased to 14 and 22 mm. In the compact produced by the 14 mm thick explosive pad, the area occupied by the central cellular structure further increased and much porosity was observed at the central region of the compact. When the explosive pad thickness was increased to 22 mm, pipe formation with much porosity and many microcracks were observed.

The microstructures across the cross-section of the compact produced in the 25 mm internal diameter aluminium tubes are shown in Fig. 7. This compact showed almost no variation in microstructure from the periphery to the centre of the compact.

4. Discussion

The impact energy imparted to the powder was calculated to be 177 $MJ\,m^{-3}$ when the 5 mm thick explosive pad was used. The structure of the compact produced using this pad (Fig. 3) reveals the well retained original dendritic structure of the initial powder almost throughout the sample, except at interparticle boundaries. Prior particle boundaries disappeared fully and no trace of particle boundaries was seen in the compact. At the triple point junctions

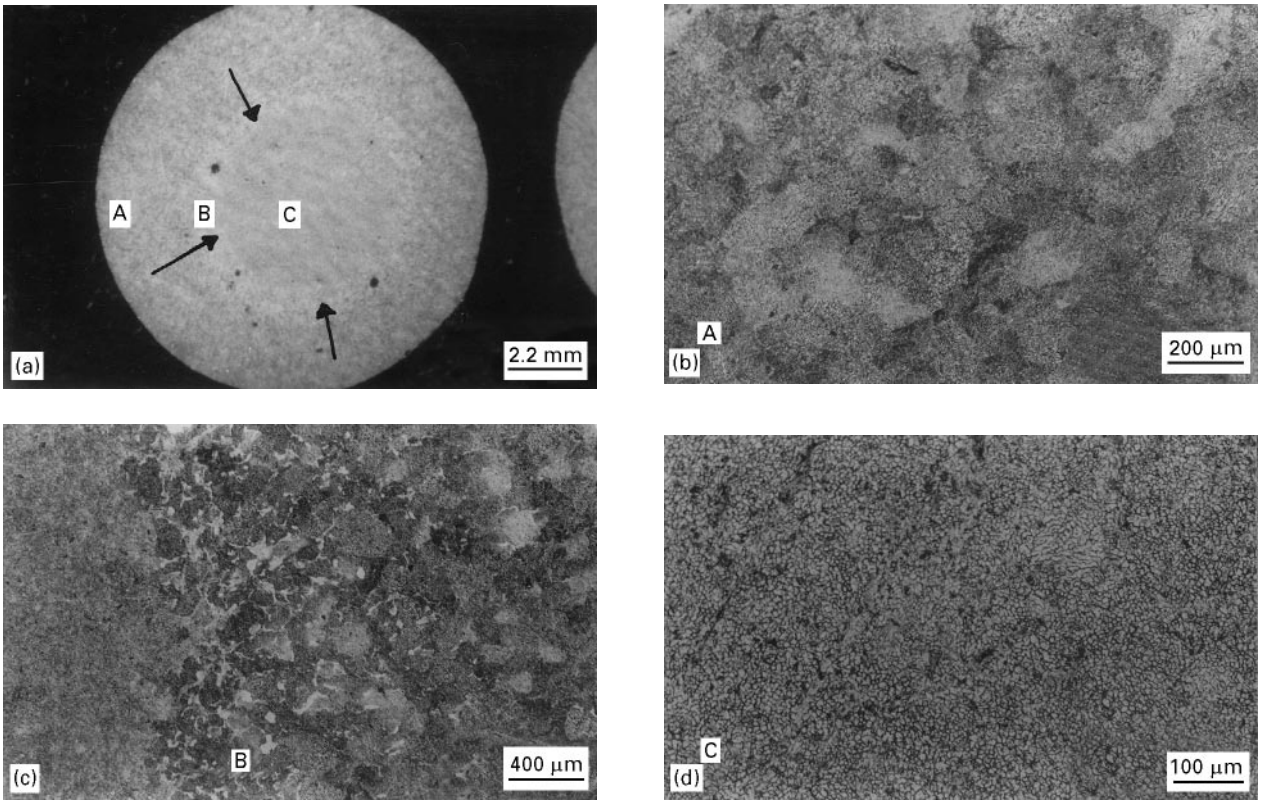

Figure 5 (a) Microstructure of the 2124 Al compact produced by a 9.5 mm thick explosive pad, showing different structures across the cross-section. (b) periphery (A), (c) middle (B), and (d) centre (C).

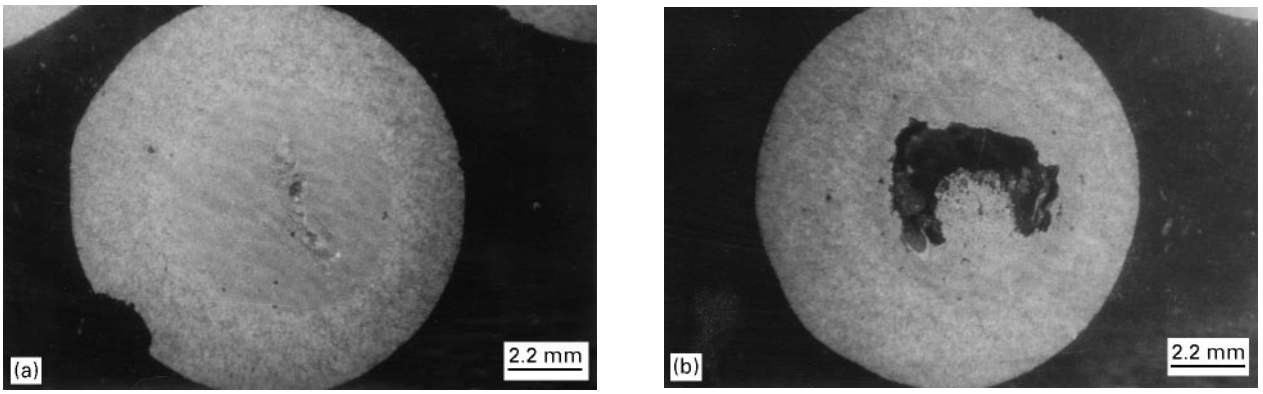

Figure 6 Porosity and pipe at the centre of the compacts produced by (a) 14 mm and (b) 22 mm thick explosive pads.

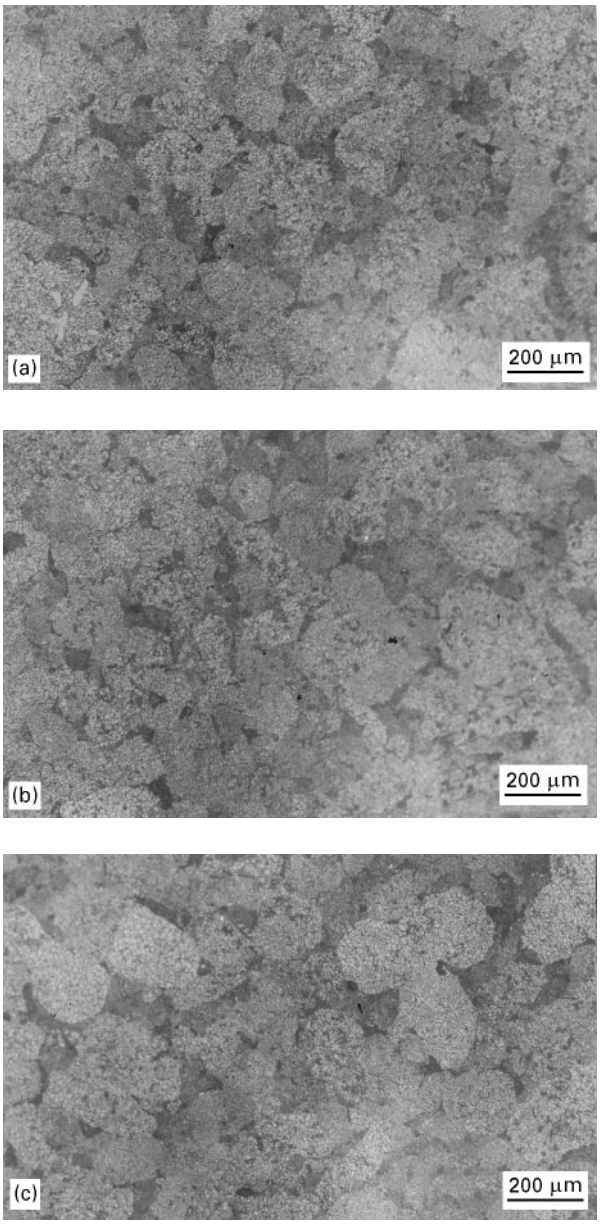

Figure 7 Microstructure of the 2124 Al compact produced in 25 mm diameter tubes showing no variation across the cross-section of the compact: (a) periphery, (b) middle and (c) centre.

we found black etched regions. The structure in these areas could not be resolved by optical microscopy. These appear to be remelted areas that could have formed due to frictional forces between the particles

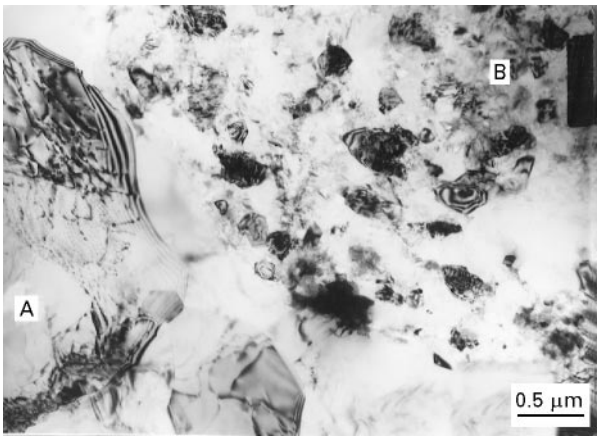

Figure 8 Bright field image of compact showing the difference in grain size between the interior of the particle (A) and the triple point junction (B).

colliding with one another at very high speeds. The fine grained microcrystalline structure of these tiny remelted regions at particle interfaces can be seen in an SEM micrograph (Fig. 4). These regions have been studied by TEM and the difference in microstructure between the particle and the triple point junction can be seen in Fig. 8. The black regions observed in the optical microscope show very fine grained structure 0.4 μm in size compared with 1.5 μm size grains at the interior of particle. Selective area diffraction of both regions clearly shows that the grains in the triple point junctions are crystalline in nature (Fig. 9).

In the central regions of the compact produced by the 5 mm thick explosive pad, the interparticle boundaries contained white non-etching areas (Fig. 3), which might have formed due to generation of high temperatures at the centre of the compact by the convergent shock waves. While the particle surfaces melt, the interiors remain relatively cool and the heat flow towards the interior could rapidly quench the melt. The cooling rates from the melt at the particle boundaries following shock consolidation, depending upon the impact energy and the amount of interparticle melting, can be as high as 10^6–10^{10} °C s [11]. This is in contrast to the cooling rates of 10^2–10^6 °C s attained in conventional rapid solidification processes [12]. Similar kinds of non-etching structures have been observed in explosively compacted Markomet

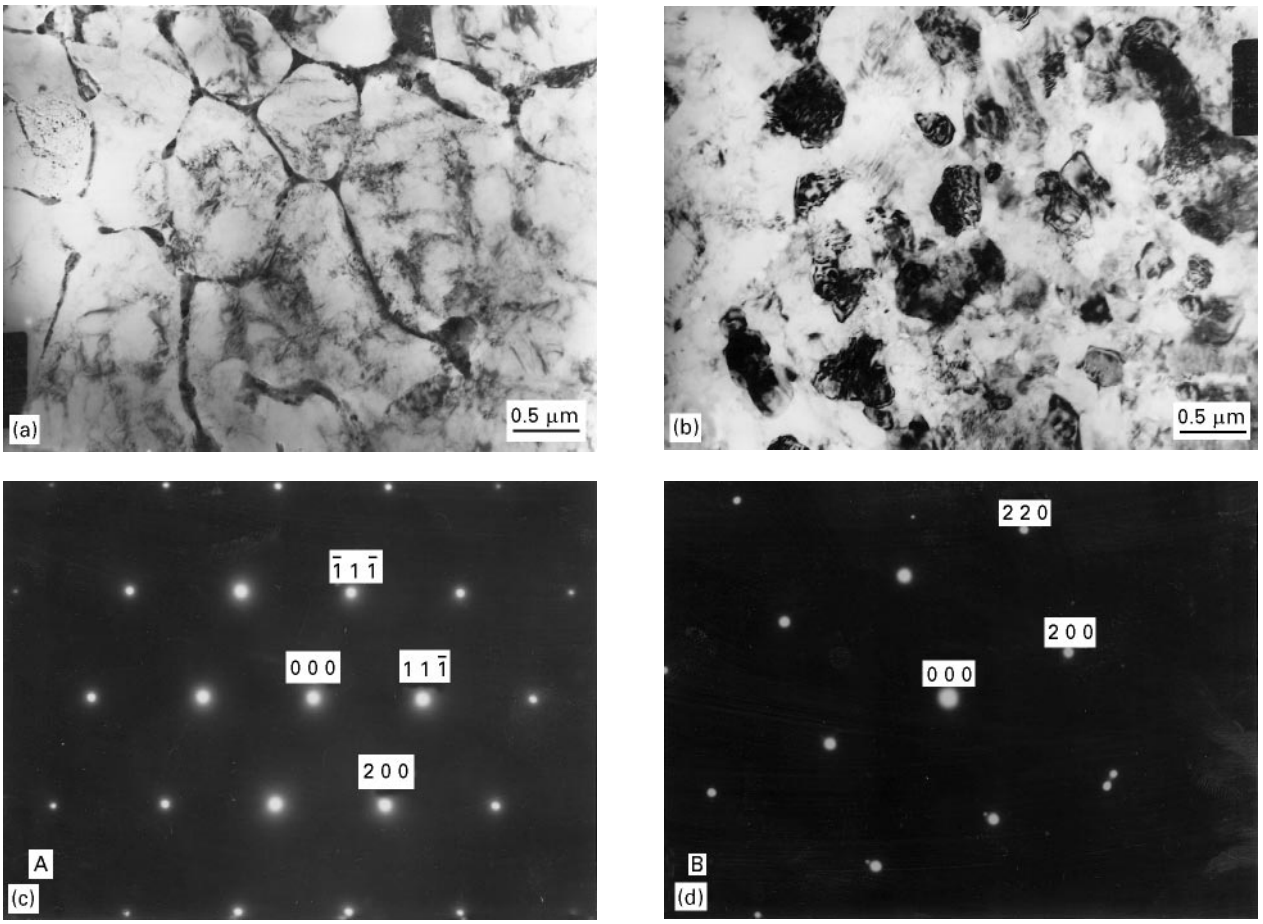

Figure 9 (a, b) Bright field TEM image and (c, d) SAD pattern of particle interior and triple point junctions, respectively showing crystallinity in both regions.

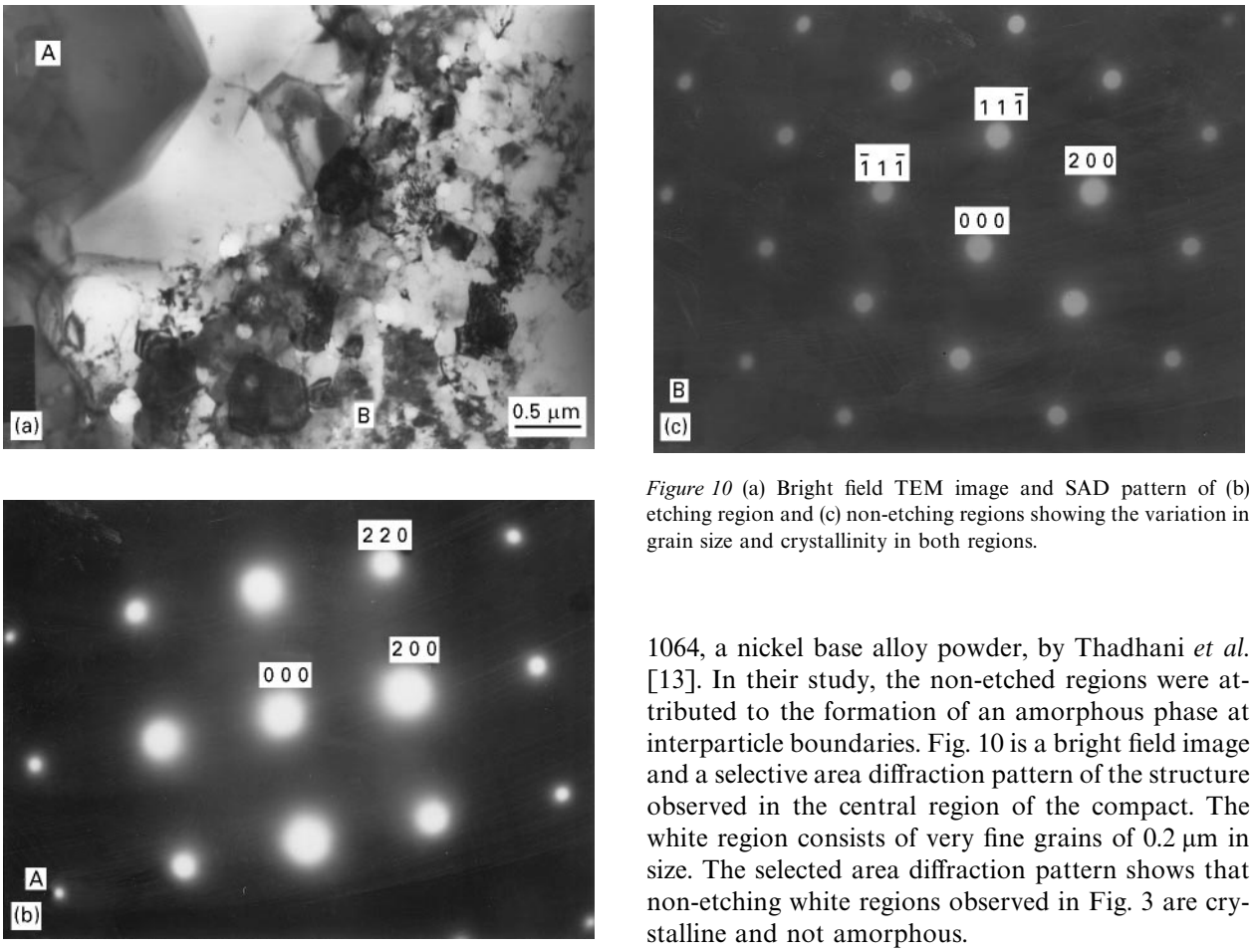

Figure 10 (a) Bright field TEM image and SAD pattern of (b) etching region and (c) non-etching regions showing the variation in grain size and crystallinity in both regions.

1064, a nickel base alloy powder, by Thadhani *et al.* [13]. In their study, the non-etched regions were attributed to the formation of an amorphous phase at interparticle boundaries. Fig. 10 is a bright field image and a selective area diffraction pattern of the structure observed in the central region of the compact. The white region consists of very fine grains of 0.2 μm in size. The selected area diffraction pattern shows that non-etching white regions observed in Fig. 3 are crystalline and not amorphous.

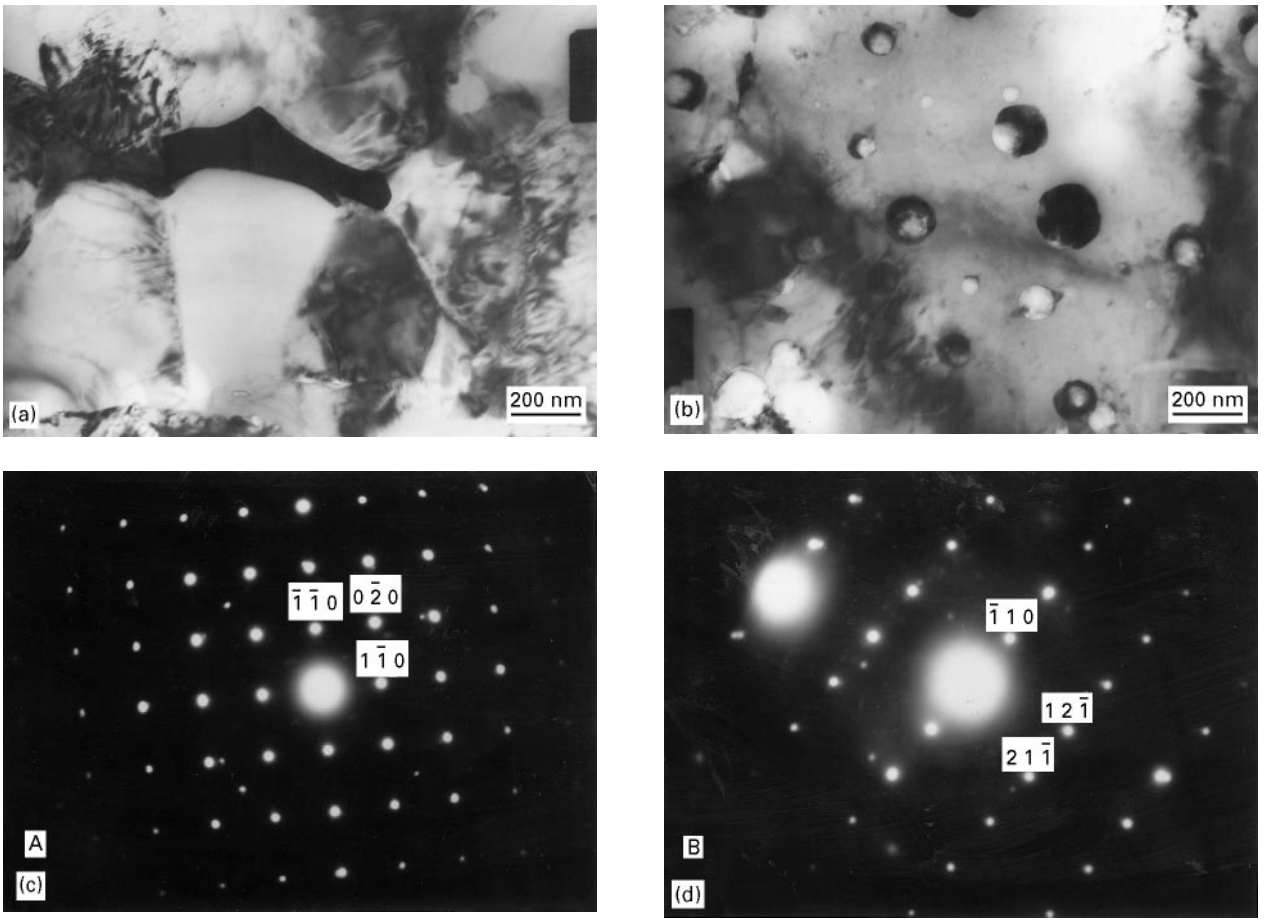

Figure 11 (a, b) Bright field TEM image and (c, d) SAD pattern of θ precipitates at intercellular region of large grains (a, c) and inside the fine grains of non-etching regions (b, d).

Interestingly, while both the original structure and the fine grained structures show θ phase precipitation, the precipitate shapes and precipitation sites are different in the two cases. In the case of particle interiors having large grained structure, the θ phase precipitated at the grain boundaries in a continuous way; whereas in the fine grained structure of white non-etching areas, it precipitated inside the grains in the form of globules. TEM imaging and selected area diffraction in Fig. 11, show the difference in appearance of the θ phase in the two regions and confirm that both are θ phase. Precipitation of the θ phase as a spherical shape inside the remelted zones could be due to additional nucleation sites that would have been created due to the very rapid solidification rates.

Three distinct microstructural regions are found in the compact produced by the 9.5 mm thick explosive pad with an imparted impact energy of 920 MJ m^{-3}; these can be explained considering the change in pressure across the cross-section. It is known that the pressure generated in axisymmetric explosive compaction will increase in order from the periphery to the centre of the compact [14]. The well bonded original dendritic structure found at the periphery can be attributed to the generation of pressure just sufficient to meet the requirement for particle bonding. As one moves radially inwards the pressure increases due to convergent shock waves. This increase in pressure could have resulted in the formation of the different microstructures observed across the cross-section of the compact. With increasing pad thickness, the location of the dual structure found at the centre of the compact using the 5 mm explosive pad, shifts radially outwards like a ring, indicating a shift in the conditions for obtaining the dual structure towards the periphery. With increased impact energy, the intensity of the shock wave will naturally increase, which results in higher pressures and temperatures at the centre of the compact. The cellular structure, present at the centre of the compact obtained using a 9.5 mm explosive pad (Fig. 5), could be due to large scale melting and resolidification caused by such high temperatures. TEM imaging shows that the central region consists of two kinds of grains: very fine equiaxed grains and longitudinal columnar grains, as shown in Fig. 12. The θ phase precipitates along the grain boundaries as shown in Fig. 13. Precipitation of the θ phase along the grain boundaries is an indication that the cooling rates in the central region of the compact produced by 9.5 mm thick explosive pad are not as high as those observed at the white non-etching areas. This could be due to the large volume involved in melting and resolidification at the central regions.

The outer regions have a hardness of 80 VPN, which is close to that of the starting material. The hardness in areas containing the white non-etching zones at the interparticle boundaries is 92 VPN. This

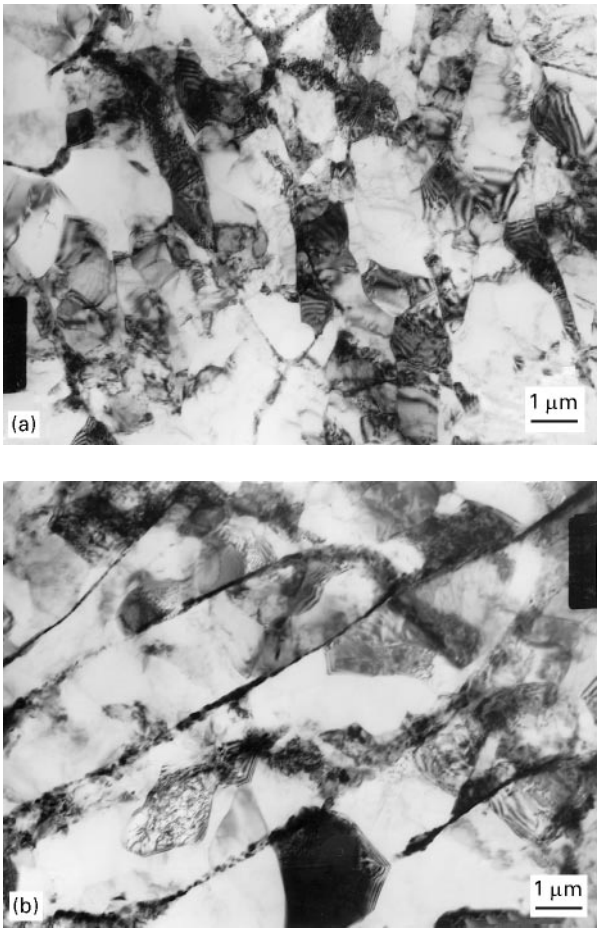

Figure 12 Bright field TEM image of the central region of the compact produced by the 9.5 mm thick explosive pad showing (a) very fine equiaxed grains and (b) longitudinal grains.

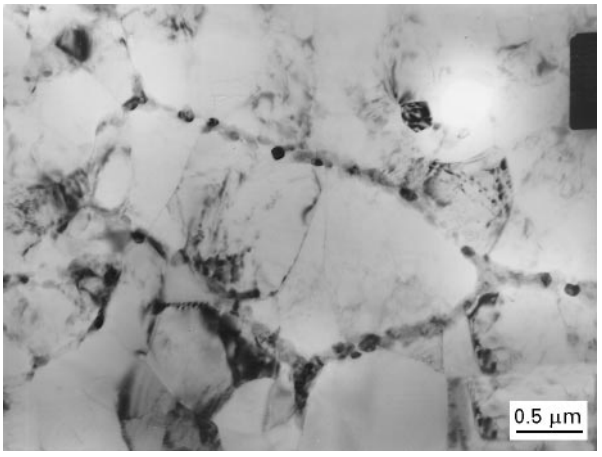

Figure 13 Bright field TEM image showing θ precipitates along the grain boundaries of equiaxed grains at the centre of the compact produced by the 9.5 mm thick explosive pad.

high hardness could be due to the very fine grain structure [7]. The low value of 58 VPN in the central region of the compact could be due to the porosity caused by melting and resolidification.

When the explosive pad thickness was increased to 14 mm and the impact energy to 2060 MJ m^{-3}, porosity appeared in the centre of the compact (Fig. 6). This could be due to the very high temperatures caused by the convergent shock waves causing high pressures [15]. The material at the centre of the compact might have melted completely and resolidified. When the explosive pad was increased to 22 mm thickness, the impact energy increased to 4545 MJ m^{-3} and the central porosity further increased leading to pipe formation due to the enlargement of the high temperature region. The locations of the dual structure, cellular structure and central pipe also shifted radially outwards.

Although compacts produced using 5 and 9.5 mm explosive pads in 11 mm diameter tubes showed microstructural variations across the cross-sections, the compacts produced using 25 mm diameter tubes with 8.5 mm explosive pads with impact energies of 220 MJ m^{-3}, showed absolutely uniform structures across the cross-sections (Fig. 7). This could be due to the availability of a longer path for the shock-waves to penetrate. When shock waves with high intensity travel from the periphery to the centre of the compact, if the length is not sufficient to absorb the entire shock energy before it reaches the centre of the compact, it raises the temperature of the interparticle boundaries thereby producing melting and resolidification of the material. This caused the variation in the microstructure across the cross-sections of the compacts produced using small size tubes.

5. Conclusions

2124 alloy powders can be compacted to 98% theoretical density by explosive compaction. Although the original microstructure is largely retained up to a 5 mm thick explosive pad with an impact energy of 177 MJ m^{-3}, the triple point junctions show refined structure. At an explosive pad of around 9.5 mm thickness and with an impact energy of 920 MJ m^{-3}, three microstructural zones are found across the cross-section. While we find original particle dendrites at the periphery of the compact, white non-etching areas are found at the interparticle boundaries at the intermediate region of the compact. Melted and resolidified porous structures are found near the centre of the compact. The white non-etching areas with very fine grains 0.2 μm in size exhibited globular precipitation inside the grain, whereas in other regions, i.e. in the interior of particles and triple point junctions, precipitation of a θ phase network was observed along the grain boundaries. The precipitation of a θ phase within the grains of the white non-etching areas seems to be the result of solidification at rates even faster than those experienced by the atomized powders. Further increases in the thickness of the explosive pad and the impact energy lead to pipe formation at the central region of the compact and shift of the other two zones towards the periphery. The problem of having a variation in microstructure can be avoided by simply increasing the diameter of the compact size while maintaining the optimum processing conditions obtained using the smaller size compacts. Thus using an optimum thickness of explosive pad, compacts up to 98% theoretical density can be prepared without degrading the rapidly solidified powder structures.

Acknowledgements

The authors wish to acknowledge Sri SLN Acharyulu, Director, D. M. R. L for his permission to publish this paper. The authors are also thankful to Mr K. K. Papukutty and Mr Soloman Raj for their help in conducting the experiments.

References

1. S. CLYENS and W. JOHNSON, *Mater. Sci. Eng.* **30** (1977) 121.
2. C. R. A. LENNON, A. K. BHALLA and J. D. WILLIAMS, *Powder Metall.* **1** (1978) 19.
3. C. F. CLINE and R. W. HOOPER, *Scripta Metall.* **11** (1977) 1137.
4. D. G. MORRIS, *Met. Sci.* **14** (1980) 215.
5. D. RAYBOULD, D. G. MORRIS and G. A. COOPER, *J. Mater. Sci.* **14** (1979) 2523.
6. *Idem*, *ibid.* **16** (1981) 589.
7. D. G. MORRIS, in "Proceedings of the International Conference on rapidly solidified materials", edited by W. Lee and R. S. Carbonara (American Society for Metals, Metals Park, OH, 1986) p. 67.
8. R. N. WRIGHT, T. E. DOYLE, J. E. FLINN and G. E. KORTH, *Mater. Sci. Eng.* **94** (1987) 225.
9. A. A. HEGAZY and T. Z. BLAZYNSKI, *Int. J. Impact Eng.* **6** (1987) 63.
10. K. SIVAKUMAR, T. BALAKRISHNA BHAT and P. RAMAKRISHNAN, *J. Mater. Process. Technol.* **62** (1996) 191.
11. D. G. MORRIS, *Met. Sci.* **16** (1982) 457.
12. M. COHEN, G. H. KEAR and R. MEHRABIAN, in Proceedings of the Second International Conference on Rapid Solidification Processing, Claitor, 1980, edited by R. Mehrabian, B. H. Kear and M. Cohen (Reston, VA, USA, March 1980) p. 1.
13. N. N. THADHANI, A. H. MUTZ, P. KASIRAJ and T. VREELAND Jr, in "Metallurgical applications of shock-wave and high-strain-rate phenomena, edited by L. E. Murr, K. P. Staudhammer and M. A. Meyers (Marcel Dekker, New York, 1986) p. 247.
14. K. P. STAUDHAMMER and K. A. JOHNSON, *ibid.* p. 149.
15. R. PRUMMER in "Explosive welding, forming and compaction", edited by T. Z. Blazynski (Applied Science Publishers, London, 1983) p. 347.

Received 20 November 1995
and accepted 2 April 1997